

Article

Modeling Hydrological Regimes of Floodplain Wetlands Using Remote Sensing and Field Survey Data

Xiaodong Na ^{1,*} and Wenliang Li ² 

¹ Key Laboratory of Remote Sensing Monitoring of Geographic Environment, College of Heilongjiang Province, Harbin Normal University, Harbin 150025, China

² Department of Geography, Environment and Sustainability, The University of North Carolina at Greensboro, Greensboro, NC 27402-6170, USA

* Correspondence: nxd@hrbnu.edu.cn

Abstract: Understanding the variations in the water regimes of wetland ecosystems is crucial to analyzing the dynamics of wetland habitats under different water management policies and recharge conditions. A MIKE21 hydrodynamic model was constructed to simulate changes in the water level and flood extent from 1 May 2014 to 9 October 2014 in the Zhalong National Nature Reserve using field measurements, a digital elevation model (DEM), radar images, and climatic, meteorological, and land-use/land-cover data. The hydrodynamic model was calibrated and validated by water levels derived from hydrological gauge stations and water level loggers and the flooding extent was derived from multi-temporal synthetic aperture radar (SAR) images in different periods to evaluate the suitability of the hydrodynamic model for simulating wetland hydrological processes. The results demonstrated that the hydrodynamic model could simulate changes in the water level and flooding of the wetlands in the entire hydrological year. Accurate simulations were obtained for both calibration and evaluation with high correlations between the simulated and observed water levels. The simulated fine-scale hydrological regimes of semi-enclosed floodplain wetlands could be used to understand the ecohydrological processes affected by different water resource allocation schemes.

Keywords: hydrodynamic model; hydrological regimes; synthetic aperture radar; wetlands



Citation: Na, X.; Li, W. Modeling Hydrological Regimes of Floodplain Wetlands Using Remote Sensing and Field Survey Data. *Water* **2022**, *14*, 4126. <https://doi.org/10.3390/w14244126>

Academic Editors: Ya Huang and Zhenhua Li

Received: 19 November 2022

Accepted: 15 December 2022

Published: 18 December 2022

Publisher's Note: MDPI stays neutral with regard to jurisdictional claims in published maps and institutional affiliations.



Copyright: © 2022 by the authors. Licensee MDPI, Basel, Switzerland. This article is an open access article distributed under the terms and conditions of the Creative Commons Attribution (CC BY) license (<https://creativecommons.org/licenses/by/4.0/>).

1. Introduction

The floodplain wetlands in Northeast China perform vital ecosystem functions and provide clean water, food, and habitats for an immense variety of species, including many endangered waterfowl species [1,2]. Although many habitat factors influence the ecological health and habitat suitability of a floodplain wetland, a key performance indicator is that the hydrological regime, including the flood extent and water depth, meets the ecological and environmental water requirements of the wetlands' flora and fauna [3]. The alteration of the catchment hydrology by human disturbance, including overexploitation of groundwater, land-use changes surrounding the wetlands, and impoundment or diversion of rivers, have put substantial pressure on wetland ecosystem functions [4]. There is an increasing need to characterize the dynamics of hydrological regimes, evaluate water shortage risks, and develop restoration plans for critical wetland ecosystems [5].

Gauge data from hydrological stations do not provide detailed records of the changes in the inundation extent or water level of floodplain wetlands due to the isolated locations, extensive areas, and high vegetation heterogeneity of wetlands. Thus, remote sensing techniques are increasingly used to map wetland distribution and flood extent in floodplain wetlands [6]. Studies have shown that a hydroperiod map based on a time-series classification of flood extent can depict seasonal flooding dynamics and the hydrological regime [7]. Meanwhile, new approaches, such as differential synthetic aperture radar interferometry (DInSAR) and distributed scatterer interferometry (DSI), have been used to map the flooding process in wetlands [8,9]. However, it is difficult to obtain long-term

ecohydrological features, such as the water depth and flooding extent, due to temporal decorrelation in time-series remote sensing data.

Several studies have modeled the inundation of wetlands at large spatial scales using advanced calculation methods and hydrological and hydrodynamic models [10,11]. For example, a large-scale distributed hydrological model (MODFLOW 2000) was used to evaluate the influences of human activities and climate change on the hydrological and ecological processes in the Okavango Delta wetlands, Botswana [12]. One-dimensional (1D) and two-dimensional (2D) MIKE FLOOD hydrodynamic models were combined to simulate daily wetland hydrological conditions in a large floodplain in Australia [13]. The hydrological and hydrodynamic models were applied to simulate floodplain inundation in the Upper Niger River Basin, a vast wetland in the Sahel Desert [14]. An enhanced quasi-2D model was established to simulate the hydrodynamics of a large wetland in the Lower Parana River Delta, Argentina [15].

Despite the wide application of hydrological and hydrodynamic models in large wetland areas, modeling wetland flooding at a fine scale is still a challenge, due to the shortage of relatively high-spatial resolution hydrological parameters [16]. Fine-scale hydrological parameters cannot be obtained from gauge records because of the inaccessibility of wetland natural reserves and data costs. Time-series data of hydrological and ecological parameters, such as inundation extent, duration, and frequency, wetland vegetation type, and vegetation canopy cover, have been obtained successfully from high-spatial resolution synthetic aperture radar (SAR) and hyperspectral imagery (HSI) [17,18]. However, these hydrological and ecological parameters have rarely been used to simulate hydrological regimes, such as the water depth and inundation extent. The simulation accuracy of hydrological regimes in a typical floodplain wetland remains to be evaluated.

In the current study, a hydrodynamic model is established to simulate the changes in the hydrological regime in the Zhalong wetland using field measurements, remote sensing images, and ancillary geographical data. The model is commonly used to simulate the daily behaviors of inflow/outflow, volume and inundation area. It has been used to investigate the water movement within the Macquarie Marshes of a large spatial scale lowland floodplain in Australia. The proposed hydrodynamic model is one of the first attempts to model the wetland hydrological regime of a semi-enclosed floodplain at a relatively high spatial resolution (30 m). The simulation results will contribute to the investigation into the impacts of recently implemented water replenishment measures on the hydrological regime and how these water management strategies have altered the habitats of endangered waterfowl species in a typical wetland natural reserve.

2. Materials and Methods

2.1. Study Area

The study area is the Zhalong wetlands located at 46°52′–47°32′ N and 123°47′–124°37′ E. The study area covers 2100 km² and is located in the temperate continental monsoon climate zone. The Zhalong wetlands are located in the inland delta of the Wuyuer River, northeast of the Songnen Plain, Heilongjiang Province, China (Figure 1). The Wuyuer River system is part of the Nenjiang river basin and runs through the Xiao Hinggan Mountains, Bei'an, Fuyu, and Qiqihar, where it flows into a lowland freshwater marsh wetland. The flooding process of the Zhalong Wetland is influenced predominantly by the Wuyuer River, whose maximum discharge occurs in the summer (August), and the Dongsheng Reservoir, whose maximum discharge occurs in the spring. Marshes represent the main land-cover type, occupying the lowland of the study areas. Reed (*Phragmites communis*) marshes comprise 80% of the vegetation community. The other marsh vegetation communities are composed primarily of *Carex meyeriana*, *Carex enervis*, and *Carex miyabei*. The wetlands provide essential breeding habitats for the red-crowned crane in Northeastern China. From 15 April to 15 May of each year, about 200 red-crowned cranes nest and hatch their eggs in the Zhalong wetlands. The flood extent, dynamics, and water level fluctuations in the

Zhalong wetlands are critical for the habitat protection of wetland vegetation communities and endangered waterfowl species.

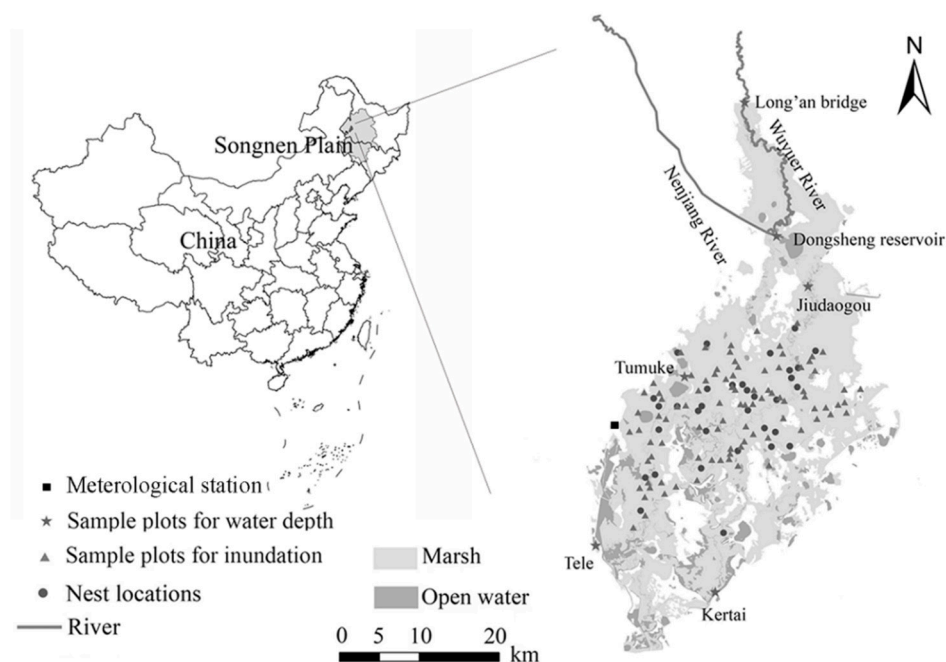


Figure 1. Location of the Songnen Plain in Northeast China (left) and the study area (right).

2.2. Data

The accuracy of the simulations used to characterize the changes in the wetland water level at a fine scale depends largely on the accuracy of the hydrological and ecological parameters, such as river runoff, inundation extent, water depth, digital topographic model, spatial distribution of vegetation communities, soil physicochemical properties, and climate data (rainfall and evaporation). The data sources, preparation, and descriptions are listed in Table 1.

Table 1. Summary of data used in the hydrodynamic models.

Type	Description	Application	Source
Topography	DEM derived from 1:10,000 topographical maps	30 m DEM for 2D elevation	Mapping and Surveying Bureau of Heilongjiang Province
Soil thematic map	1: 50,000 soil-type map with hydraulic properties	To obtain soil infiltration parameters	Heilongjiang Geography [19]
Land-cover thematic map	2014 land-cover map derived from Radarsat-2 and Landsat-8 imagery	To develop the hydraulic roughness map for the 2D model	Land cover thematic map [20]
Climate data	Rainfall, temperature and evaporation	Input parameters	Daily data set of ground climate data in China (V3.0) in 2014.
River gauge records	Includes water levels and river discharge at the Long'an Bridge station, Dongsheng Reservoir, Kertai, and Tele	River gauge records were used to define the inflow and outflow boundaries	Onset HOBO U20-001-01 water level logger, Hydrology Bureau of Heilongjiang Province, China
Wetland gauge records	Includes water levels and water temperature in 2014 in Tumuke and Jiudaogou	Wetland gauge records were used to calibrate and validate the hydrodynamic models.	Onset HOBO U20-001-01 water level logger and Thermochron@iButton temperature sensors.

Table 1. Cont.

Type	Description	Application	Source
Flood extent map	Inundation maps were derived from time-series Radarsat-2 SAR images	To calibrate and evaluate the hydrodynamic models	Flood extent map [20]
Field data	Obtained from 150 sample sites; include inundation levels and geographic coordinates	To evaluate the accuracy of flooding extent	Field survey conducted on 22 May, 2014

2.3. Model Description

A physically based, spatially distributed hydrodynamic model for the marshes (MIKE FLOOD) was developed at the Denmark Hydraulic Institute (DHI). MIKE FLOOD is a comprehensive software toolbox for floodplain modeling that combines the dynamic coupling of the one-dimensional river model MIKE 11 and two-dimensional MIKE 21 model systems. The flow module in the MIKE 21 model is commonly utilized to simulate hydrological regimes in wetlands, lakes, estuaries, coastal areas, and oceans. It can simulate changes in the water level and flow caused by various factors, including sources and sinks, evaporation, bottom friction stress, wind shear stress, and flooding and drying boundaries. Stratification of wetlands is not considered in the model. The module simulates the unsteady flow in two horizontal directions based on the principles of the conservation of mass and momentum [21]. A network of interconnected grids is discretized [22]. The governing equations (Saint-Venant equation) were utilized to describe the flow of water between the cells [23]. This method has been successfully used to simulate the impact of climate change and dams on the hydrological regime and connectivity of large floodplain wetlands [24].

2.4. Model Parameters

This study simulated the inundation extent, water depth, and flow connection between water bodies in the Zhalong wetlands using the MIKE 21 hydrodynamic module. The input parameters included the boundary conditions (inflows and outflows), topographical features derived from a digital elevation model (DEM), precipitation, evaporation, surface infiltration rate, hydraulic roughness, and eddy viscosity. The outputs included a time-series of water depth distribution and horizontal flow maps.

A spatial resolution of 30 m was selected to obtain the detailed hydrological regime, which is a key habitat feature used to assess the habitat suitability for the breeding red-crowned cranes in the Zhalong NNR. The area of the model domain was 2100 km², and the area of the input variables was 1200 × 1900 cells. The model domains were divided based on the hydrological and topographic features of the study area and were a function of the watershed partition by the hydrological analysis module in ArcGIS 10.1. Two upstream inflows (Wuyuer River and Dongsheng Reservoir) are the main water sources of the Zhalong wetlands. Water flow and water depth data were obtained from the Long'an Bridge gauge station in the upstream region of the Wuyuer River and the Dongsheng Reservoir, a water diversion project, to determine the boundary inflows. The water depths in the downstream region of the Zhalong wetlands (Tele and Kertai) were derived from Onset HOBO water level loggers for an entire hydrological year to represent the boundary outflows. Daily rainfall and evaporation were obtained from the Ground Climate Data of China (V3.0). Recently collected soil field survey data were used to calculate the infiltration rate [25]. Time-series remote sensing data, including Radarsat-2 and Landsat 8 imagery, were used to map changes in land-use and land-cover types and the inundation extents in the wetlands. The land-use and land-cover types included meadows, marshes, open water, bare soil, and cultivated land. Initial roughness values were assigned to the different land-cover types using Manning's roughness coefficient derived from the published literature [26]. The values were improved during the calibration.

2.5. Model Calibration and Evaluation

As we can observe from the flowchart of the model calibration and evaluation (Figure 2), the measured water stage data derived from the Onset HOBO data loggers and the flood extent maps derived from the time-series Radarsat-2 imagery were utilized to calibrate the hydrodynamic model. The MIKE 21 model has been calibrated against two flow events at Tumuke and Jiudaogou, comprising a low-flow event (1 May 2014–22 May 2014) and a high-flow event (10 June 2014–7 July 2014) (Table 2). During the calibration, the initial conditions of the Manning coefficients were manually adjusted to reproduce the observed inundation extent and recorded water levels at Tumuke and Jiudaogou. Figure 3 presents the calibrated Manning coefficients for different land-cover types. The Manning coefficients are comparable to the values listed in previous publications [27,28].

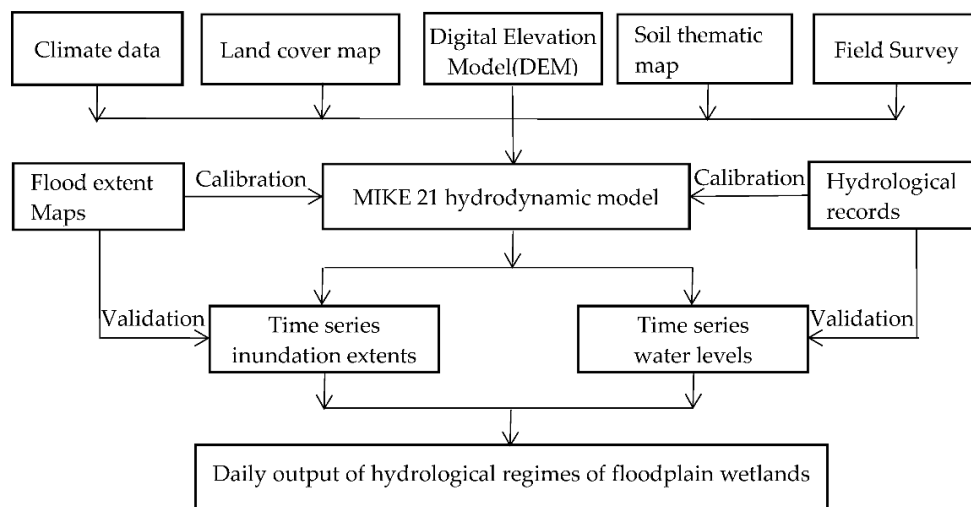


Figure 2. Flowchart of the calibration and validation process used to build the hydrodynamic model.

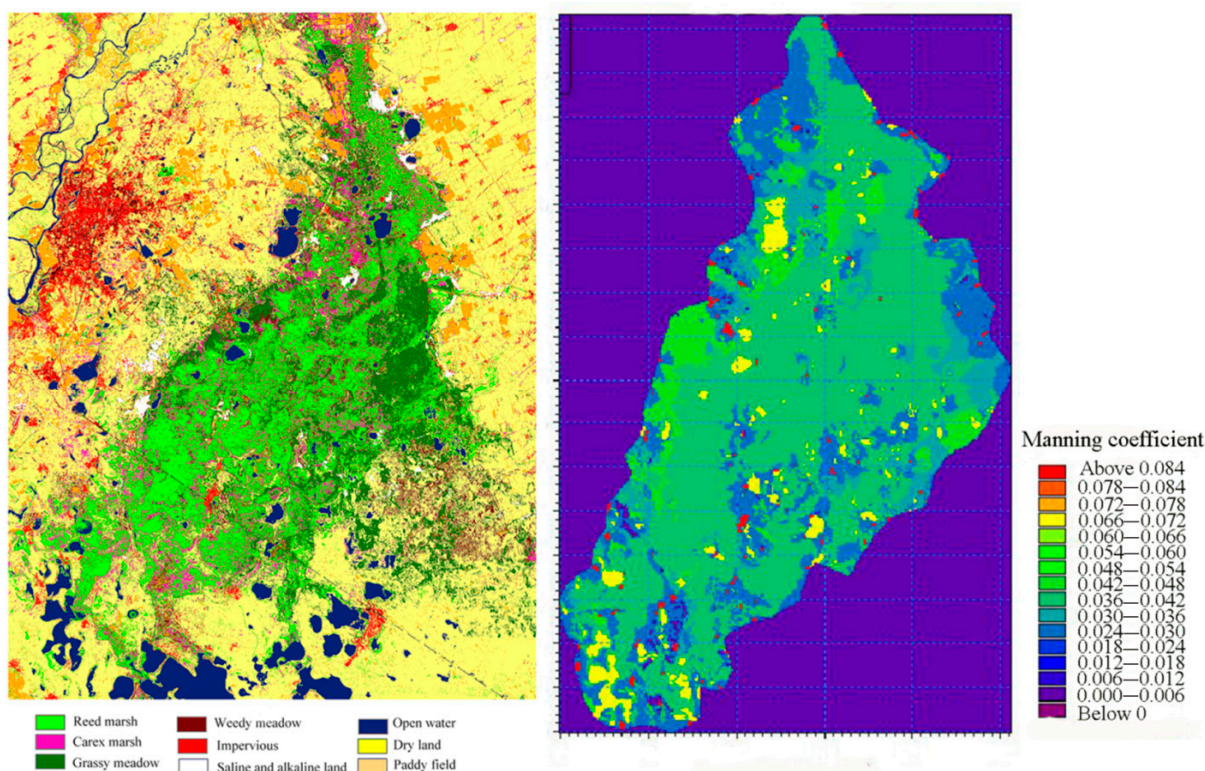


Figure 3. Land-cover map (left) and calibrated Manning coefficients (right).

Table 2. Historical flooding events used for MIKE 21 hydrodynamic model calibration.

Event Location	Start Date	End Date	Inundation Map Dates	Use
Tumuke	1 May 2014	29 May 2014	1 May 2014, 22 May 2014	Calibration
Tumuke	10 June 2014	7 July 2014	10 June 2014, 6 July 2014	Calibration
Tumuke	15 July 2014	20 August 2014	24 July 2014, 17 August 2014	Validation
Tumuke	6 September 2014	6 October 2014	10 September 2014, 2 October 2014	Validation
Jiudaogou	1 May 2014	29 May 2014	1 May 2014, 22 May 2014	Calibration
Jiudaogou	10 June 2014	7 July 2014	10 June 2014, 6 July 2014	Calibration
Jiudaogou	15 July 2014	20 August 2014	24 July 2014, 17 August 2014	Validation
Jiudaogou	6 September 2014	6 October 2014	10 September 2014, 2 October 2014	Validation

The flood mapping method using Radarsat-2 images (8 m resolution) and Landsat 8 OLI images has been described in our previous study [20]. The wetland vegetation and inundation levels were measured in a field survey conducted on 22 May 2014. Data from 150 sampling sites were used to evaluate the classification accuracy of the flood extent derived from the Radarsat-2 images and the hydrodynamic model. The sampling sites were well dispersed to prevent autocorrelation (Figure 1). An error matrix was used to calculate the user's accuracy, producer's accuracy, overall accuracy, and kappa coefficients. Two evaluation metrics, Pearson's coefficient of determination (R^2) and Nash–Sutcliffe efficiency (NSE), were calculated to calibrate and validate the MIKE 21 hydrodynamic model. R^2 indicates the degree of similarity between the simulated and observed water levels, and the NSE assesses the goodness of fit of the hydrological model [29]. The calibrated MIKE 21 model was further validated against two more flow events at the same places, including high (24 July 2014–17 August 2014) and medium flow (10 September 2014–2 October 2014) (Table 2). The duration of these events covers the full range of flow conditions in the Zhalong wetlands.

3. Results

3.1. Simulation of Water Levels

The calibration and evaluation results for the three hydrological conditions (extremely dry period, peak of the storm period, and flood recession period) are listed in Table 3. The R^2 and NSE indicated the very good fit of the model in the calibration period and a lower but acceptable fit in the evaluation periods. The simulated and observed water levels at the gauge stations for the evaluation periods are shown in Figure 4.

Table 3. The evaluation indicators of MIKE 21 for water levels within the Zhalong wetlands.

Locations	Calibration (1 May 2014–29 May 2014) Low Flow		Calibration (1 June 2014–7 July 2014) High Flow		Validation (6 September 2014–4 October 2014) Medium Flow		Validation (15 July 2014–12 August 2014) High Flow	
	R^2	NSE	R^2	NSE	R^2	NSE	R^2	NSE
Tumuke	0.96	0.95	0.95	0.94	0.95	0.86	0.85	0.83
Jiudaogou	0.97	0.96	0.96	0.95	0.93	0.92	0.89	0.81

Note(s): R^2 and NSE were selected as performance indicators (Henriksen et al., 2008). $R^2 \geq 0.85$ and $NSE \geq 0.75$: very good; $0.85 > R^2 \geq 0.65$ and $0.75 > NSE \geq 0.65$: good; $0.65 > R^2 \geq 0.5$ and $0.65 > NSE \geq 0.5$: satisfactory; $R^2 < 0.5$ and $NSE < 0.5$: poor.

The observed water levels were highly consistent with the simulated levels at the Tumuke and Jiudaogou gauge stations. In addition, we did not observe systematic bias between the simulated and observed water levels. The simulation results were more accurate during the flood recession period than during the peak of the storm period. The low accuracies of the simulated water levels were partly caused by missing inflow data for the Shuangyang River during the peak of the storm period. Therefore, this discrepancy will be corrected if we can accurately estimate the missing inflow that occur at the peak of the

storm period. The simulation provides an approach for calculating the probable maximum flooding extent and water level, which are essential in assessing the ecosystem resistance and resilience to extreme hydrological events in a wetland.

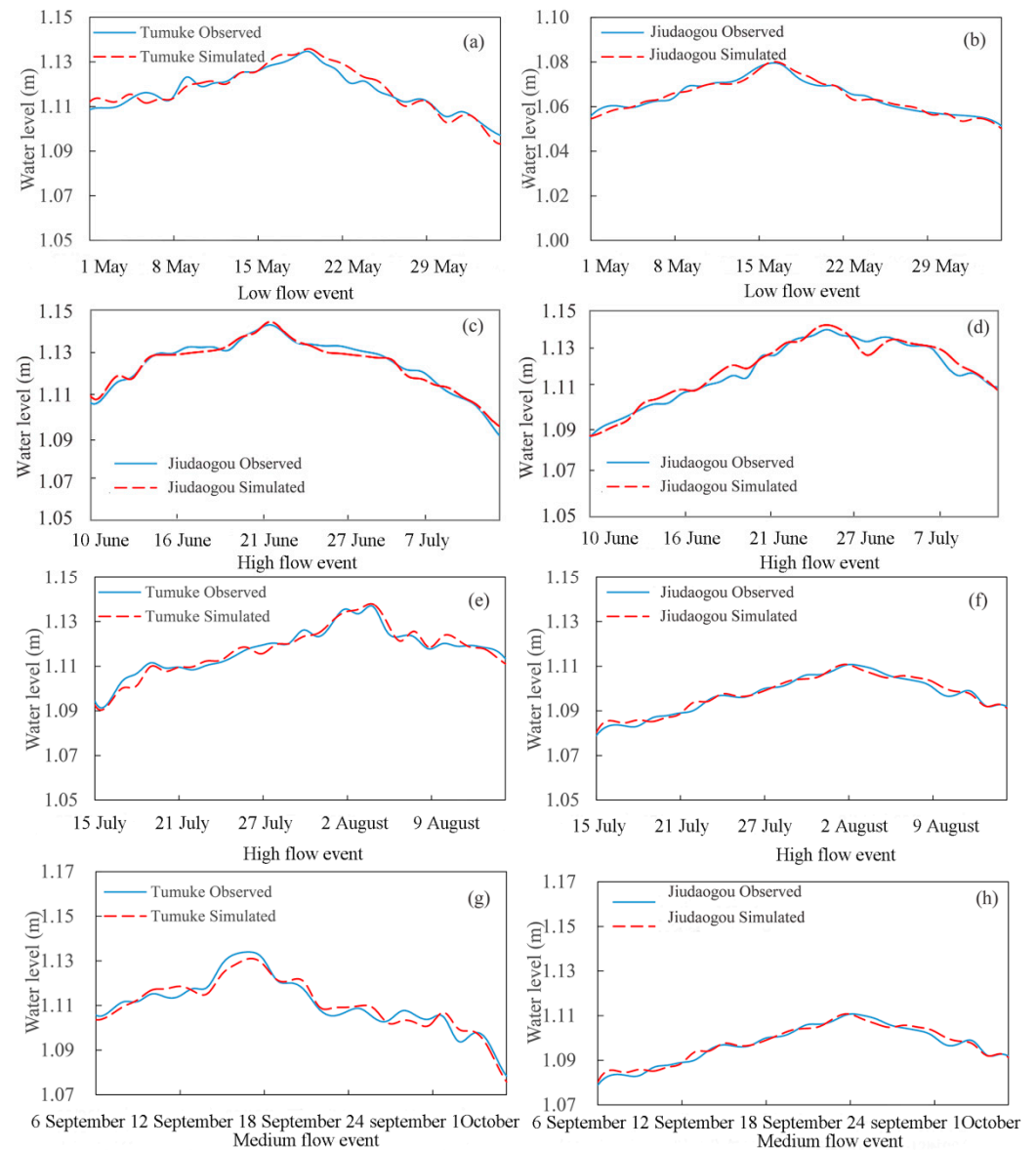


Figure 4. Simulated and observed water levels at Jiudaogou and Tumuke for the calibration and evaluation periods. Water levels during May 2014 in the calibration period (a,b), water levels from June to July 2014 in the calibration period (c,d), water levels from July to August 2014 in the evaluation period (e,f), and water levels in September 2014 in the evaluation period (g,h).

3.2. Simulation of Inundation Extent

The comparison of the inundation extent derived from the hydrodynamic model and remote sensing imagery is shown in Figure 5. The accuracy assessment results are listed in Table 4. The simulated flood extent of the MIKE 21 hydrodynamic model was similar to the classification results derived from remote sensing imagery for different hydrological periods (Figure 5). The classification results derived from Radarsat-2 images had a higher overall accuracy (94.3%) and kappa coefficient (0.91) than the result obtained from the hydrodynamic model (87.86% and 0.83, respectively). The hydrodynamic model tended to underestimate the flood extent in the peak flow event, as indicated by the lower producer's accuracy (81.16%) and the higher omission error (18.84%) (Table 4). This discrepancy was

likely caused by the underestimation of the inflow used as the input parameter of the hydrodynamic model, rather than the low predictive ability of the model.

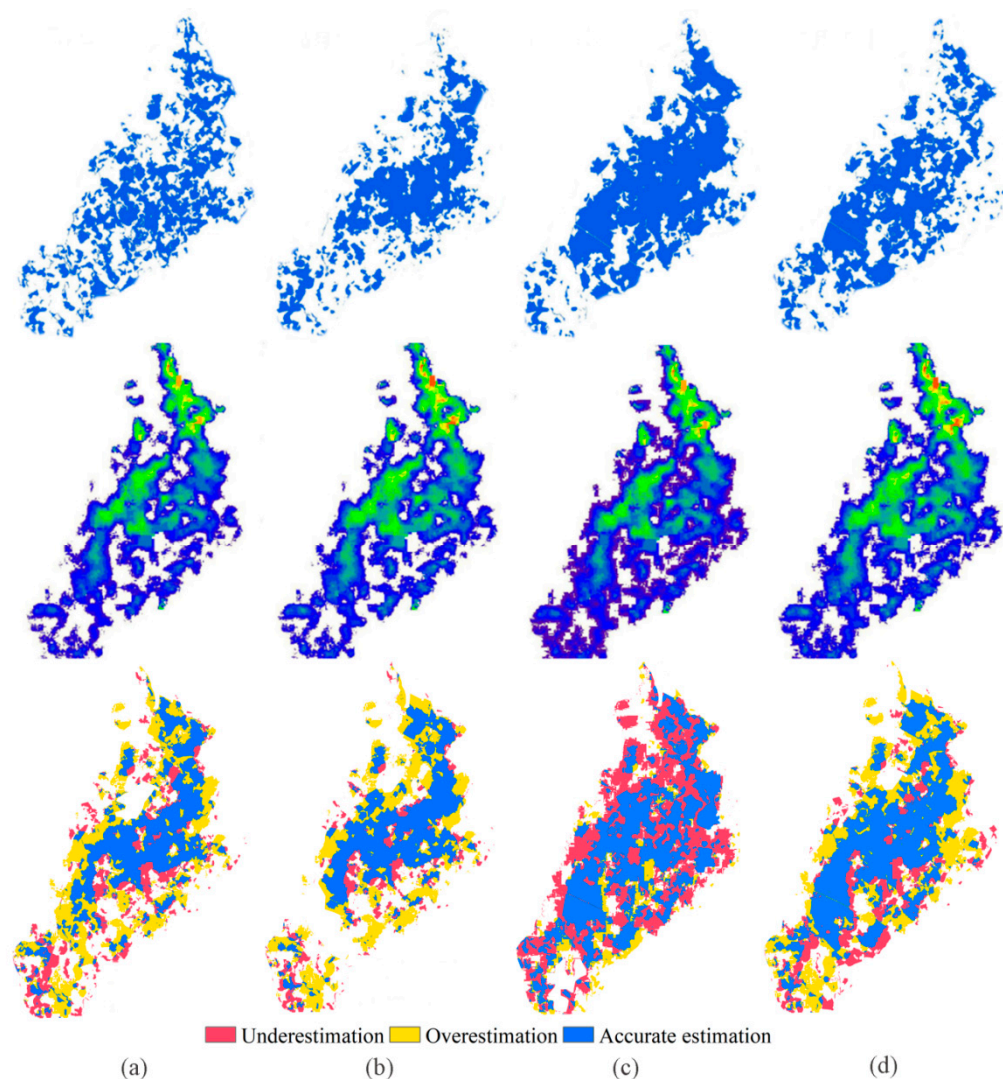


Figure 5. The flood extent derived from remote sensing data (**top**), the hydrodynamic model (**middle**) and the difference in inundation extents between the model and remote sensing observations for the (a) extremely dry period (1 May 2014), (b) flooding period (22 May 2014), (c) peak of the storm period (24 July 2014), and (d) flood recession period (10 September 2014).

Table 4. Accuracy assessment of the flood extent derived from remote sensing data and hydrodynamic model in the Zhalong wetlands.

Flood Extent	User's Accuracy		Producer's Accuracy		Overall Accuracy	Kappa
	Flooded	Non-Flooded	Flooded	Non-Flooded		
Remote sensing imagery	99.88	90.50	93.79	99.55	94.30	0.91
Hydrodynamic model	97.70	72.02	81.16	87.15	87.86	0.83

4. Discussion

We established a MIKE21 hydrodynamic model using water level data from field measurements, climate, meteorological, land-use/land-cover, and topographical data, as well as multi-source remote sensing imagery, to simulate water level changes in a typical floodplain wetland. The objective was to understand the dynamics of wetland hydrological

regimes for different upstream inflows to enable the development of reasonable water replenishment strategies for wetland reserves. The model's ability to simulate flood dynamics in delta wetlands must be evaluated to represent hydrological and hydraulic processes. Most of the previous calibrations and evaluations of distributed hydrodynamic models have been performed using observed water levels, due to the lack of other geospatial data [15]. In the current study, the hydrodynamic model was calibrated by combining the flood extents derived from multi-temporal Radarsat-2 SAR images with the observed water levels. The simulation results of the flood extent dynamics in the watershed are consistent with the flood extent dynamics derived from multi-temporal Radarsat-2 SAR images, indicating the suitability of the proposed hydrodynamics model for simulating the hydrological regime in a floodplain wetland.

Manning's roughness coefficient is commonly used for validating hydrodynamic models and affects the accuracy of the simulation results. In general, the hydraulic roughness of the Zhalong wetlands, as defined by Manning's n , depends on the wetland vegetation type [30]. This study assigned distributed Manning's n values to the 13 vegetation communities in the wetland vegetation maps, which are derived from optical, radar, and ancillary topographical data [26]. The initial value of Manning's n values is typically in the range of 0.01 (bare ground) to 0.01 (dense vegetation cover). In the calibration process, Manning's n values were manually adjusted by increasing and decreasing these parameters by 20% to reproduce the observed inundation extent and recorded water levels. Higher simulation accuracy is achieved using the calibrated distributed Manning's n values than the global Manning's n values because it considers the spatial heterogeneity of hydraulic roughness in the flood plain. The impacts of different Manning's n values on the water level in the wetland were evaluated by a sensitivity analysis. It was found that a slight change in Manning's coefficient significantly affected the simulated water level, which is consistent with the results of Wester et al. (2018) [15].

Cultivated lands and residential lands are rapidly expanding around the Zhalong wetlands. These land-cover types require infrastructure development, including dike and drainage construction, which has disconnected the wetland from water inflow, resulting in a water shortage condition. Fewer water resources due to human disturbance and climate change have changed the hydrological pattern and ecological structure of the Zhalong wetland ecosystem [4]. As a result, the water depth in the wetlands has decreased, causing a decline in the water quality of the wetland ecosystem. Water replenishment measures have been implemented in the Zhalong National Nature Reserve to maintain wetland functions and protect the habitat of endangered waterfowl species. However, the impacts of water management strategies on the hydrological regime and waterfowl habitat have not yet been quantitatively assessed. Both the quantity and timing of water replenishment could not be quantified due to the inaccessibility of the wetland and the water level dynamics.

This wetland provides important breeding habitats for rare waterfowl species, such as *Grus japonensis* and *Ciconia boyciana* [31]. Unlike in situ monitoring and remote sensing methods, the proposed MIKE 21 hydrodynamic model could accurately simulate the spatial and temporal dynamics of the water levels in the flood plain of the wetland for different supplemental flows from the upstream Dongsheng Reservoir. However, we also noticed that only the water levels over an entire hydrological year could be used to calibrate and validate the model in the current study, due to the scarcity of the field data in the wetlands. Additional monitoring for the water levels during the low-flow hydrological years should be taken to evaluate the performance of the hydrodynamic model under multi-year drought conditions. The results would help to assess the response of the endangered waterfowl habitats to the hydrological regimes during the extreme drought events and provide reasonable water management strategies for the wetland reserves.

5. Conclusions

This study investigated the hydrological regime of the Zhalong wetlands in the western Songnen Basin, China. Hydrological data on the water level, flood extent, and flood

duration are critical for understanding the ecological patterns and hydrological processes of the wetlands. The accuracy evaluation results based on the gauged water levels indicated that the performance of the fine-scale MIKE 21 hydrodynamic model was acceptable. The R^2 ranged from 0.85 to 0.96, and the NSE ranged from 0.81 to 0.95. Calibration and validation of the model against field records and remote sensing images demonstrated that the model could accurately simulate the water levels and inundation extents in the wetland area. In summary, wetland recharge should consider the recharge time and changes in the wetland hydrological conditions. This research demonstrates the feasibility of simulating water levels in wetlands at a fine scale and provides a foundation for selecting and optimizing wetland management strategies. In a future study, we will combine the hydrodynamic model with a habitat suitability assessment model to analyze the impact of different water management strategies on wetland flooding and habitat suitability for endangered waterfowl species.

Author Contributions: X.N. and W.L. designed the experiments; X.N. performed the field survey and analyzed the data; X.N. wrote the paper. All authors have read and agreed to the published version of the manuscript.

Funding: This work was supported by the Natural Science Foundation of Heilongjiang Province, China (Grant No. YQ2020D005) and the Young Scientists Fund of the National Natural Science Foundation of China (Grant No. 41001243).

Conflicts of Interest: The authors declare no conflict of interest.

References

1. Bian, H.F.; Yan, T.T.; Zhang, Z.X.; He, C.G.; Sheng, L.X. Mapping deciduous broad-leaved forested swamps using ALOS/Palsar data. *Chin. Geogra. Sci.* **2016**, *26*, 352–365. [[CrossRef](#)]
2. Mitsch, W.J.; Gosselink, J.G. The value of wetlands: Importance of scale and landscape setting. *Ecol. Econ.* **2000**, *35*, 25–33. [[CrossRef](#)]
3. Webb, J.A.; Wallis, E.M.; Stewardson, M.J. A systematic review of published evidence linking wetland plants to water regime components. *Aqua. Bot.* **2012**, *103*, 1–14. [[CrossRef](#)]
4. Na, X.D.; Zang, S.Y.; Zhang, N.N.; Cui, J. Impact of land use and land cover dynamics on Zhalong wetland reserve ecosystem, Heilongjiang Province, China. *Int. J. Environ. Sci. Technol.* **2015**, *12*, 445–454. [[CrossRef](#)]
5. Schulte, M.L.; McLaughlin, D.L.; Wurster, F.C.; Balentine, K.; Speiran, G.K.; Aust, W.M.; Stewart, R.D.; Varner, J.M.; Jones, C.N. Linking ecosystem function and hydrologic regime to inform restoration of a forested peatland. *J. Environ. Manag.* **2019**, *233*, 342–351. [[CrossRef](#)]
6. Na, X.D.; Zang, S.Y.; Wu, C.S.; Li, W.L. Mapping forested wetlands in the Great Zhan River Basin through integrating optical, radar, and topographical data classification techniques. *Environ. Monit. Assess.* **2015**, *187*, 696. [[CrossRef](#)] [[PubMed](#)]
7. Huang, C.; Chen, Y.; Wu, J.P. Mapping spatio-temporal flood inundation dynamics at large river basin scale using time-series flow data and MODIS imagery. *Int. J. Appl. Earth Obs.* **2014**, *26*, 350–362. [[CrossRef](#)]
8. Xie, C.; Xu, J.; Shao, Y.; Cui, B.S.; Goel, K.; Zhang, Y.J.; Yuan, M.H. Long term detection of water depth changes of coastal wetlands in the Yellow River Delta based on distributed scatterer interferometry. *Remote Sens. Environ.* **2015**, *164*, 238–253. [[CrossRef](#)]
9. Yin, J.; Zhao, Q.; Yu, D.P.; Lin, N.; Kubanek, J.L.; Ma, G.Y.; Liu, M.; Pepeg, A. Long-term flood-hazard modeling for coastal areas using InSAR measurements and a hydrodynamic model: The case study of Lingang New City, Shanghai. *J. Hydrol.* **2019**, *571*, 593–604. [[CrossRef](#)]
10. Arega, F. Hydrodynamic modeling and characterizing of Lagrangian flows in the West Scott Creek wetlands system, South Carolina. *J. Hydro-Environ. Res.* **2013**, *7*, 50–60. [[CrossRef](#)]
11. Felder, G.; Zischg, A.; Weingartner, R. The effect of coupling hydrologic and hydrodynamic models on probable maximum flood estimation. *J. Hydrol.* **2017**, *550*, 157–165. [[CrossRef](#)]
12. Milzow, C.; Burg, V.; Kinzelbach, W. Estimating future ecoregion distributions within the Okavango Delta Wetlands based on hydrological simulations and future climate and development scenarios. *J. Hydrol.* **2010**, *381*, 89–100. [[CrossRef](#)]
13. Wen, L.; Macdonald, R.; Morrison, T.; Hameed, T.; Saintilan, N.; Ling, J. From hydrodynamic to hydrological modelling: Investigating long-term hydrological regimes of key wetlands in the Macquarie Marshes, a semi-arid lowland floodplain in Australia. *J. Hydrol.* **2013**, *500*, 45–61. [[CrossRef](#)]
14. Fleischmann, A.; Siqueira, V.; Paris, A.; Collischonn, W.; Paiva, R.; Pontes, P.; Crétaux, J.F.; Bergé-Nguyen, M.; Biancamaria, S.; Gosset, M.; et al. Modelling hydrologic and hydrodynamic processes in basins with large semi-arid wetlands. *J. Hydrol.* **2018**, *561*, 943–959. [[CrossRef](#)]
15. Wester, S.J.; Grimson, R.; Minotti, P.G.; Booij, M.J.; Brugnach, M. Hydrodynamic modelling of a tidal delta wetland using an enhanced quasi-2D model. *J. Hydrol.* **2018**, *559*, 315–326. [[CrossRef](#)]

16. Yeo, I.Y.; Lang, M.W.; Lee, S.; McCarty, G.W.; Sadeghi, A.M.; Yetemen, O.; Huang, C.Q. Mapping landscape-level hydrological connectivity of headwater wetlands to downstream waters: A geospatial modeling approach-Part 1. *Sci. Total Environ.* **2019**, *653*, 1546–1556. [[CrossRef](#)]
17. Logah, F.Y.; Amisigo, A.B.; Obuobie, E.; Kankam-Yeboah, K. Floodplain hydrodynamic modelling of the Lower Volta River in Ghana. *J. Hydrol.* **2017**, *14*, 1–9. [[CrossRef](#)]
18. Yang, Y.Z.; Wu, Q.B.; Jin, H.J.; Wang, Q.F.; Huang, Y.D.; Luo, D.L.; Gao, S.H.; Jin, X.Y. Delineating the hydrological processes and hydraulic connectivities under permafrost degradation on Northeastern Qinghai-Tibet Plateau, China. *J. Hydrol.* **2019**, *569*, 359–372. [[CrossRef](#)]
19. Zang, S.Y. *Heilongjiang Province Geography*; Beijing Normal University Publishing Group: Beijing, China, 2014; pp. 123–126.
20. Na, X.D.; Zang, S.Y.; Wu, C.S.; Tian, Y.; Li, W.L. Hydrological Regime Monitoring and Mapping of the Zhalong Wetland through Integrating Time Series Radarsat-2 and Landsat Imagery. *Remote Sens.* **2018**, *10*, 702. [[CrossRef](#)]
21. Dutta, D.; Alam, J.; Umeda, K.; Hayashi, M.; Hironaka, S. A two dimensional hydrodynamic model for flood inundation simulation: A case study in the Lower Mekong River basin. *Hydrol. Process.* **2007**, *21*, 1223–1237. [[CrossRef](#)]
22. Cunge, J. Two dimensional modelling of flood plains. In *Unsteady Flow in Open Channels*; Mahmood, K., Yevjevich, V., Eds.; Water Resources Publications: Fort Collins, CO, USA, 1975; pp. 705–762.
23. Warren, I.R.; Bach, H.K. MIKE 21: A modelling system for estuaries, coastal waters and seas. *Environ. Softw.* **1992**, *7*, 229–240. [[CrossRef](#)]
24. Karim, F.; Dutta, D.; Marvanek, S.; Petheram, C.; Ticehurst, C.; Lerat, J.L.; Kim, S.; Yang, A. Assessing the impacts of climate change and dams on floodplain inundation and wetland connectivity in the wet–dry tropics of northern Australia. *J. Hydrol.* **2015**, *522*, 80–94. [[CrossRef](#)]
25. Mo, B.; Chen, X.Y.; Yang, Y.C.; Luo, B.L.; Tang, J.; Gong, C.M.; Lin, Z.H.; Zhou, T.J.; Shen, Y.K. Research on soil infiltration capacity and its influencing factors in different land uses. *Res. Soil Water Conserv.* **2016**, *23*, 13–17.
26. Wang, J.J.; Zhang, K.D.; Gong, J.G.; Fan, Y.; Xu, D. Overland flow resistance law under different vegetation coverage. *J. Soil Water Conserv.* **2015**, *29*, 1–6.
27. Nash, J.E.; Sutcliffe, J.V. River flow forecasting through conceptual models part I—A discussion of principles. *J. Hydrol.* **1970**, *10*, 282–290. [[CrossRef](#)]
28. Piedra-Cueva, I.; Fossati, M. Residual currents and corridor of flow in the Rio de la Plata. *Appl. Mathemat. Model.* **2007**, *31*, 564–577. [[CrossRef](#)]
29. Biancamaria, S.; Bates, P.D.; Boone, A.; Mognard, N.M. Large-scale coupled hydrologic and hydraulic modelling of the Ob river in Siberia. *J. Hydrol.* **2009**, *379*, 136–150. [[CrossRef](#)]
30. Bowen, S.; Simpson, S. *Changes in Extent and Condition of the Vegetation Communities of the Macquarie Marshes Floodplain 1991–2008*; Environment Department of New South Wales: Sydney, Australia, 2010.
31. Na, X.D.; Zhou, H.T.; Zang, S.Y.; Wu, C.S.; Li, W.L.; Li, M. Maximum Entropy modeling for habitat suitability assessment of Red-crowned crane. *Ecol. Indic.* **2018**, *91*, 439–446. [[CrossRef](#)]